# Preparation and Thermal Characterization of Nanographene-Enhanced Fatty Acid-Based Solid-Liquid Organic Phase Change Material Composites for Thermal Energy Storage

Ragul Kumar Kittusamy* – Velavan Rajagopal – Paul Gregory Felix

PSG College of Technology, Department of Mechanical Engineering, India

*In this research work, nano-phase change material (NPCM) composites were prepared by adding 1 %, 2 %, and 3 % mass fractions of highly conductive carbon-based graphene nanoparticles into the base phase change material (PCM). The existence and uniform graphene dispersion in the PCM was confirmed through Raman spectrometer and scanning electron microscope (SEM) analysis. The Fourier transform infrared (FTIR) and x-Ray diffraction (XRD) results showed that all three NPCM composites were chemically stable, and their crystallinity was similar to the base PCM. For the sample with 3 % graphene, the solid-state thermal conductivity was increased by 219.89 %, and liquid-state thermal conductivity was increased by 161.65 %, with a 3.52 % drop in latent heat capacity was revealed from differential scanning calorimetry (DSC) analysis. All NPCM composites have onset and peak melting temperatures closer to the base PCM. Hence, the NPCM composites can be employed for thermal energy storage (TES) integrated solar water heater (SWH) applications.*

Keywords: phase change material, graphene nanoparticles, nano-phase change material composite, thermal energy storage, solar water heater

**Highlights**
- *Highly conductive nanographene was dispersed into the fatty acid-based PCM.*
- *The prepared NPCM composites were thermally and chemically stable.*
- *For 3 wt.% graphene in PCM, the solid-state thermal conductivity was improved by 219 %.*
- *The DSC result shows a 3.52 % decline in latent heat capacity for NPCM 3 composite.*
- *All NPCM composites have closer onset and peak melting temperatures with base PCM.*

## 0 INTRODUCTION

Solar energy is an essential sustainable resource since it is available in abundance. Considering the absorption and scattering losses, the total solar flux reaching the earth's surface is about 1.08 GW. Hence, the earth's surface receives $3.4 \times 10^{24}$ J of total energy annually, roughly around 7500 times the annual world primary energy use [1]. As a tropical country, India receives about 5000 trillion kWh of solar radiation annually, resulting in a daily average solar irradiance of 4 kWh/m² to 7 kWh/m². Currently, the residential sector contributes roughly about 84 % of India's total solar water heater (SWH) installations. Solar water heating is a recognized technology for cleaner hot water production from solar energy. A 100-litre SWH system can prevent up to 1.5 tonnes of $CO_2$ emissions each year [2].

However, the insolation of solar radiation at any point on the earth's surface is diurnal. It depends on several factors, such as weather conditions, length of the day, latitude, and season at that particular surface [3]. Therefore, it requires a technology that stores the heat energy received from the sun during sunshine hours and uses it for off-shine hours. Thermal energy storage (TES) technology is an attractive option for storing solar energy effectively to reduce the mismatch between energy supply and demand [4].

Integrating phase change material (PCM) based latent heat thermal energy storage (LHTES) in SWH is an environment-friendly solution for passively obtaining additional hot water with the same system capacity. Using PCMs in TES systems has proliferated and received tremendous attention worldwide [5] and [6]. Generally, PCMs, including organic, inorganic, and organic-inorganic categories, exhibit good potential for storing energy in the form of sensible and latent heat. The PCM-based LHTES can absorb and release substantial energy during the phase transition process at near isothermal working conditions [7].

Domestic solar water heating falls under low and medium-temperature applications with an operating temperature of around 65 °C [8]. Among the PCMs, paraffin wax was widely used for TES in SWHs, typically having a melting temperature range between 50 °C to 60 °C, a latent heat capacity of 200 kJ/kg, and a solid-state thermal conductivity of 0.172 W/(m·K) [9] to [11]. With paraffin as an energy storage medium for TES in SWHs, the maximum water temperature obtained from SWHs has been limited to 60 °C,

despite the heat energy supplied to TES being at an elevated temperature. This temperature limitation is due to the heat energy stored in paraffin PCM beyond 60 °C is in the form of sensible heat, which is inferior to the latent heat stored at 60 °C. Using appropriate PCM with melting temperatures close to the operating temperature of SWH is necessary to obtain hot water at the desired temperature. It has been identified that the proper selection of PCM melting temperature plays a crucial role in the performance of TES systems [12]. This constitutes a research gap that could be bridged by utilizing alternative PCMs to paraffin, possessing a higher melting temperature than 60 °C.

The eutectic mixture of fatty acids offers a more comprehensive range of engineering applications because of its greater heat storage reliability [13]. Therefore, some recent studies on the synthesis and characterization of fatty acids and their eutectic mixtures reported that the fatty acid-based PCMs are a potential candidate for TES applications [14] and [15]. The fatty acid-based PCMs fall under the organic category, and they have attracted broad attention in the field of TES applications. Compared to individual fatty acid PCMs, the eutectic combinations of organic fatty acids significantly impact the phase change temperature. Any desired phase transition temperature for the TES application could be obtained by proper mixing of two or more PCMs, forming a eutectic mixture of fatty acids. For the eutectic mixture, the melting temperature of the selected PCMs should be around the desired operating temperature range such that each component in the mixture melts and solidifies simultaneously [16].

In contrast, the thermal conductivity of widely used contemporary PCMs in LHTES systems is relatively low, typically ranging from 0.5 W/(m·K) to 1 W/(m·K), which prolongs the melting and solidification process of the PCM used in TES applications. This phenomenon seriously affects the overall efficiency of the TES system. Therefore, it is necessary to address this issue with potential heat transfer enhancement techniques [17].

The inclusion of smaller mass fractions of highly conductive metallic or carbon-based nanoparticles in a PCM significantly improves the effective thermal conductivity of PCM, leading to accelerated charging and discharging rates of PCM [18]. The nanoparticles have a greater surface-area-to-volume ratio. By increasing the mass concentration of nanoparticles in the base PCM, the thermal conductivity of PCM could be improved with a decrease in the latent heat of the PCM. Hence, the mass/volume fraction of nanoparticles added to the PCM is optimized to obtain the lowest possible reduction in latent heat capacity [19].

For the previous two decades, the heat transfer enhancement in PCM-based TES applications by employing metal-based nanoparticles has been the subject of extensive research. Many researchers are currently focusing on carbon-based nano-additives (multi-wall carbon nanotubes, graphene nanoparticles, and nano-graphite) to enhance the effective thermal conductivity of PCM [20]. For the same mass fraction, metal-based nanoparticles have a higher mass-to-volume ratio when compared to carbon-based nanoparticles. Hence, this could reduce the effect of nanoparticles in PCM due to the aggregation and sinking of metal particles inside the liquid phase-change medium [21].

The use of graphene nanoparticles in energy storage and thermal management applications has been put in practice, and it outmatches metal nanoparticles, carbon-based nanotubes, and other carbon allotropes [22]. It has been proved that adding nanographene to PCM improves its thermal conductivity and, at the same time, increases the viscosity of PCM, leading to the degradation of the effect of natural convection in its liquid state. As a result, compared to pure PCM, the temperature rise rate of nano-graphene-based PCM composites was more significant during the initial stage and lowered during later stages of the charging process [23]. The higher the mass fraction of graphene in PCM, the higher the viscosity of the liquid nano-phase change material (NPCM) composite. Hence, this was a limiting factor for adding higher mass concentrations of graphene in PCM to retain the liquid state temperature rise rate of NPCM composites [24].

This study addresses the aforementioned research gaps by using a new eutectic fatty acid-based solid-liquid organic PCM and graphene nanoparticles as a thermal conductivity booster. The PCM used in this study is selected based on its melting temperature by considering the operating temperature of the domestic SWH. The main objective of this research work is to prepare and characterize the thermal properties of the NPCM composites, considering their applicability for TES integrated domestic SWHs. The appropriate use of the prepared NPCM composites and the design of the LHTES system for practical applications requires basic knowledge about the material characteristics.

## 1 METHODS

The research strategy followed in this work consists of three modules: material selection,

preparation of NPCM composites, and characterization of the samples.

## 1.1 Material Selection

The base PCM, OM65, which is a mixture of organic fatty acids, was purchased from Pluss Advanced Technologies Pvt. Ltd., Haryana, India. PCM selection was made by considering the applicability to LHTES for domestic SWHs. At room temperature, the PCM appeared to be a white flake solid. The highly conductive graphene nanoparticles were purchased from Ultrananotech Pvt. Ltd., Bangalore, India. The physical appearance of graphene was that of a light black fluffy powder. All the materials were used exactly as they were procured, with no further modifications. The suppliers' properties of PCM and nanographene are listed in Table 1.

## 1.2 Preparation of NPCM Composites

The NPCM composites were prepared using a two-step mechanical dispersion method [25] and [26], as illustrated in Fig. 1. The PCM was heated up to 80 °C (above its melting temperature), and the liquid PCM was stirred at 600 rpm using a hot plate magnetic stirrer. The graphene nanoparticles were then added to the liquid PCM in mass fractions of 1 wt.%, 2 wt.%, and 3 wt.% and stirred continuously for 1 hour to obtain NPCM 1, NPCM 2, and NPCM 3 samples, respectively.

**Table 1.** *Properties of PCM and graphene nanoparticles*

| PCM (OM65) | | Graphene | |
|---|---|---|---|
| Melting temperature [°C] | 65 | Purity [%] | > 99 |
| Solid specific heat, 30 °C [kJ/(kg·K)] | 2.83 | Particle diameter [nm] | 5 to 10 |
| Latent heat [kJ/kg] | 204 | Length [$\mu$m] | 5 to 10 |
| Solid density, 30 °C [kg/m³] | 924 | Density [g/cm³] | 3.1 |
| Solid thermal conductivity @ 30 °C [W/(m·K)] | 0.18 | Surface area [m²/g] | 200 to 210 |
| Liquid thermal conductivity @ 70 °C [W/(m·K)] | 0.13 | Thermal conductivity [W/(m·K)] | 3000 |

The graphene concentration in PCM was limited to 3 wt.% by considering a minimum reduction in latent heat capacity of the NPCM composite [27]. The macro-level dispersion of nanoparticles in PCM with some agglomerated particles was obtained by shear mixing using magnetic stirring. The liquid NPCM was subjected to ultrasonication for 1 hour by maintaining water bath temperature at 80 °C and sonication frequency at 40 kHz [28]. The dispersion

quality was improved by ultrasonication, thus by untangling the agglomerated graphene nanoparticles, which are collapsed by microbubbles inside the liquid medium, forming a homogeneous composite. The homogeneously dispersed liquid NPCM samples were then allowed to solidify entirely at room temperature before being collected for characterization. After complete solidification, the samples are turned into cake-like composites, subsequently ground into powder for characterization by using a polished granite mortar and pestle.
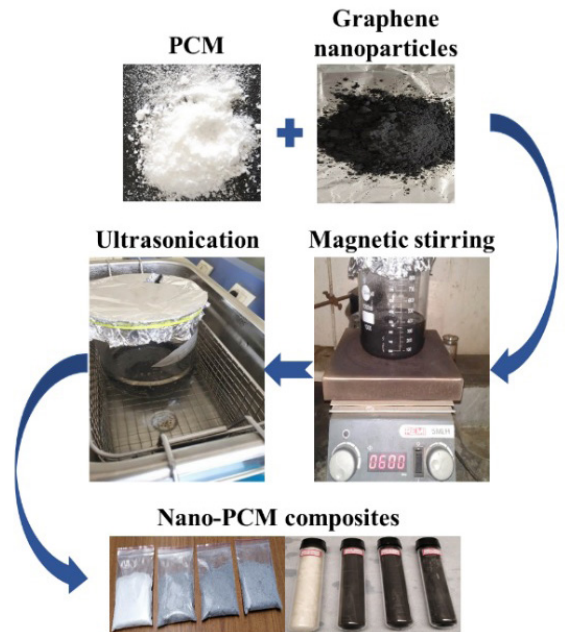


**Fig. 1.** *Schematic of NPCM composite preparation by the two-step method*

## 1.3 Characterization of the Samples

The presence of graphene in the prepared samples was identified using a WITec alpha 300 Raman spectrometer with a 532 nm argon green laser source. A scanning electron microscope (SEM) (ZEISS EVO 18, USA) with 10 kV accelerated voltage was used to examine the dispersion of graphene in PCM and the microstructures of all the prepared samples at a working distance of 10 mm. The chemical interaction between graphene nanoparticles and PCM was investigated using a Shimadzu IRAffinity 1 s model Fourier transform infrared spectrometer (FTIR) with a wavenumber range from 4000 cm⁻¹ to 400 cm⁻¹ and a resolution of 0.5 cm⁻¹. The Empyrean, Malvern Panalytical multipurpose X-ray diffractometer (XRD) with Cu K$\alpha$ ($\lambda$ = 1.54 Å) as an X-Ray source was used to study the crystal structures of PCM and NPCM

3 in the range of $0° \leq 2\theta° \leq 80°$ at a scanning rate of 6 s⁻¹. Thermal conductivities of PCM and NPCM composites were measured at solid state and liquid state using a TEMPOS thermal analyser (METER Group). The energy storage properties, such as melting temperature, latent heat capacity, and thermal decomposition temperature of PCM and NPCM composites were characterized using a NETZSCH STA 2500 Regulus analyser, a simultaneous differential scanning calorimetry-thermogravimetry analysis (DSC-TGA) instrument by heating the samples from 30 °C to 200 °C in an alumina crucible, and in an $N_2$ environment at a 10 °C/min heat ramp.

## 2 RESULTS AND DISCUSSION

### 2.1 SEM Analysis

The dispersion quality and microstructure of the prepared samples were examined through SEM. It can be seen from Fig. 2a that the graphene nanoparticles have rough flake-shaped multiple layered structures with wrinkles and wrapped edges. This characteristic feature indicates the presence of small random porous structures in graphene that can hold a small quantity of PCM in it. In comparison with the same mass concentration of metal nanoparticles, the carbon-based graphene with random void structures accommodates a smaller volume of liquid PCM, resulting in a minimum reduction in the latent heat capacity of the TES system. The typical graphene nanoparticle width was approximately 6.5 μm, indicating the graphene nanoparticles' larger aspect ratio. Fig. 2b to d shows the microstructures of NPCM 1, NPCM 2, and NPCM 3 composites comprising 1 wt.%, 2 wt.%, and 3 wt.% of the porous structured graphene nanoparticles in the base PCM. The solidified NPCM composites morphologies appear rougher, and uniformly distributed graphene in the base PCM was identified. More numerous rough protuberances were observed on the samples as the nanoparticle concentration increased, ensuring the graphene's strong embedment in crystal PCM, and establishing effective heat conduction paths within the NPCM composites [29].

### 2.2 Raman Spectra Analysis

A Raman spectrometer is commonly used to characterize carbon compounds because the strong Raman intensities were observed for conjugated carbon and carbon-carbon complexes [30]. The presence of graphene in all the NPCM composites was
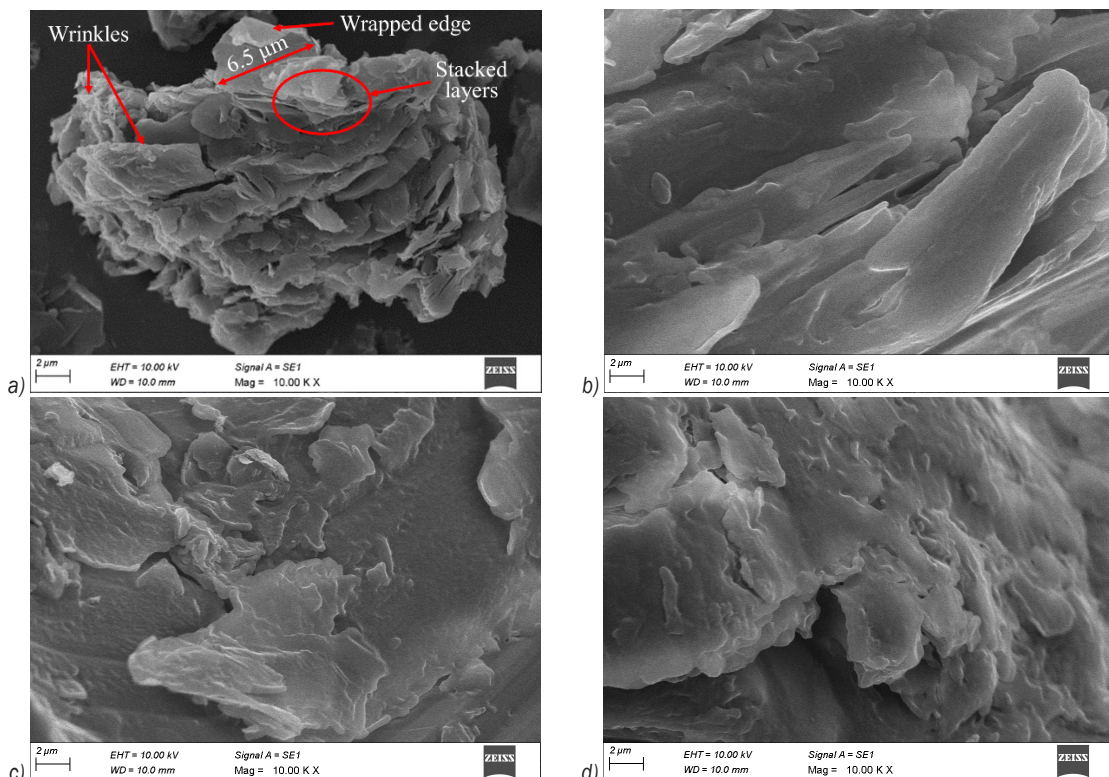


**Fig. 2.** *SEM images of: a) graphene, b) NPCM 1, c) NPCM 2 and, d) NPCM 3*

analysed using a Raman spectrometer, as illustrated in Fig. 3. The graphene nanoparticle shows two strong peaks: a D peak at 1357 cm^{-1} and a G peak at 1594 cm^{-1}. The D band corresponds to the sp³ hybrid carbon atoms, the defect band whose intensity is directly related to the defect in the sample. A weak D band peak was seen for the graphene employed in this study, indicating that the graphene quality was acceptable. The G band is sharp, and the band is an in-plane vibrational mode involving the sp² hybridized carbon atoms contained in the graphene sheets [31]. The Raman spectrum of all three NPCM composites comprised D peak and G peak at its corresponding wavelength, as shown in Fig. 3. Thus, the presence of graphene in all NPCM composites was confirmed. The inclusion of graphene into the base PCM resulted in modifications in some spectral peaks of PCM and the formation of new characteristics in the spectra, implying that only the vibrational modes were modified due to the attachment of the graphene flakes in the chains of fatty acid PCM [32].
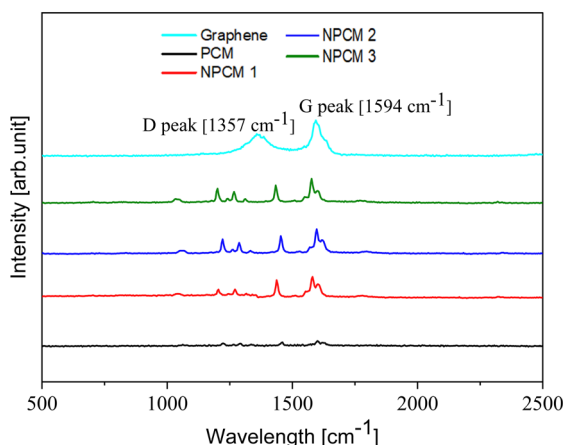


**Fig. 3.** *Raman spectra of graphene, PCM, and NPCM composites*

### 2.3 FTIR Analysis

The chemical characteristics of the fatty acid PCM, graphene nanoparticles, and NPCM composites are portrayed in Fig. 4. The peaks near 2920 cm^{-1} and 2850 cm^{-1} wavelengths indicate the stretching vibrations of the symmetric –CH$_3$ and –CH$_2$– groups of long-chain fatty acids. The absorption band of aliphatic C–H stretching vibration generally overlaps with the absorption band of O–H stretching vibration between the wavelength 3000 cm^{-1} and 2750 cm^{-1}. The peak at 1700 cm^{-1} represents the stretching vibrations of –C=O. The peak at 1470 cm^{-1} represents the –CH$_2$ and the peak at 1300 cm^{-1} represents the C–H and C–C groups bending peak. It was observed that

the characteristic peaks of the PCM and the NPCM composites were similar, indicating that the chemical structures of the PCM remain unchanged upon blending it with graphene nanoparticles. Therefore, all the prepared NPCM composites were in a chemically stable form.
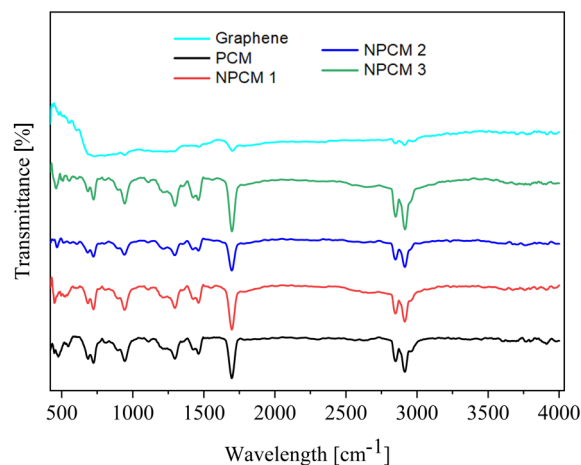


**Fig. 4.** *FTIR spectra of Graphene, PCM, and NPCM composites*

### 2.4 XRD Analysis

The PCM and NPCM 3 composite phase structure was characterized by XRD analysis. As illustrated in Fig. 5, the diffraction pattern of PCM includes two strong peaks at 21.54º and 24.12º, corresponding to the diffraction of (110) and (021) crystal planes of the fatty acid mixtures. Also, the XRD result of PCM shows a few weak diffraction peaks, such as the peak at 11.1º and 20.45º, as a result of the diffraction of (005) and (–111) crystal planes of PCM, respectively. It can be seen that the XRD pattern of the NPCM 3 composite is similar to the PCM diffraction pattern, revealing that the graphene insertion does not affect the crystal structure of the base PCM. Therefore, it was clear that the graphene-enhanced PCM composites are a mere physical mixture of PCM and graphene, and their crystal structures remained unaltered. From the above XRD results of the sample having 3 wt.% graphene (NPCM 3), it was inferred that the untested samples having 1 wt.% and 2 wt.% graphene in PCM (NPCM 1 & NPCM 2) are also a physical mixture of the PCM and the graphene.

### 2.5 Thermal Conductivity Measurement

The variation of solid and liquid state thermal conductivity of the PCM and the NPCM composites with change in mass fraction of the graphene

nanoparticles is shown in Fig. 6. It was observed that when the mass concentration of graphene nanoparticles increases, so does the thermal conductivity of PCM composites. The percentile increase in the thermal conductivity of the NPCM composites compared to PCM is summarized in Table 2. The solid-state thermal conductivity of the NPCM 1 composite was 0.39 W/(m·K), measured at 30 ºC, with an increase of 113.2 % over the base PCM. The solid-state thermal conductivity of NPCM 2 and NPCM 3 composites was increased by 173.48 % and 219.89 % with 2 wt.% and 3 wt.% graphene in the base PCM. The liquid-state thermal conductivity of NPCM 1, NPCM 2, and NPCM 3 composites was enhanced by 75.94 %, 134.59 %, and 161.65 %, respectively, as compared to the base PCM ($k_{PCM}$ at 70 ˚C is 0.13 W/(m·K)).
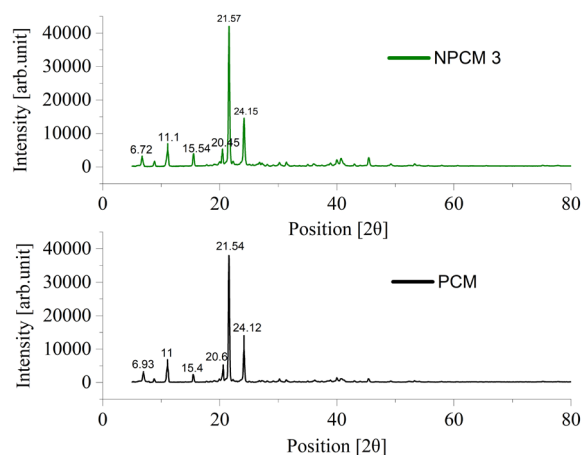


Fig. 5. *XRD patterns of PCM and NPCM 3 composite*
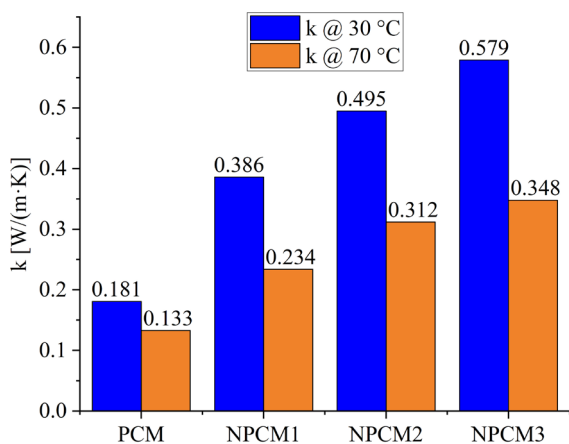


**Fig. 6.** *Thermal conductivity of PCM, and NPCM composites*

The percentile increase in the thermal conductivity of the NPCM composites tends to decline with a further rise in the graphene concentration.

This trend was attributed to the phenomenon called agglomeration of the nanoparticles in liquid PCM [33], which occurs in NPCM composites with higher concentrations of nanoparticles. Hence, the phenomenon mentioned above was another reason for restricting the graphene mass added in PCM to 3 wt.%. With a further increase in the mass concentration of nanoparticles in PCM, there may not be a proportional improvement in the thermal conduction paths created by nanoparticles inside the NPCM composite.

### 2.6 DSC-TGA Analysis

Fig. 7 represents the DSC curves of PCM and NPCM composites. It was observed that the DSC curves of the NPCM composites were consistent with that of the base PCM, with a sharp solid-liquid phase transition and a modest decline in the heat flow peak for every 1 wt.% increase in the graphene concentration. Therefore, the above observation indicates that all the prepared NPCM composites were thermally stable. The latent heats of corresponding peaks were calculated by integration method considering the peaks above the baseline using NETZSCH Proteus thermal analysis software.
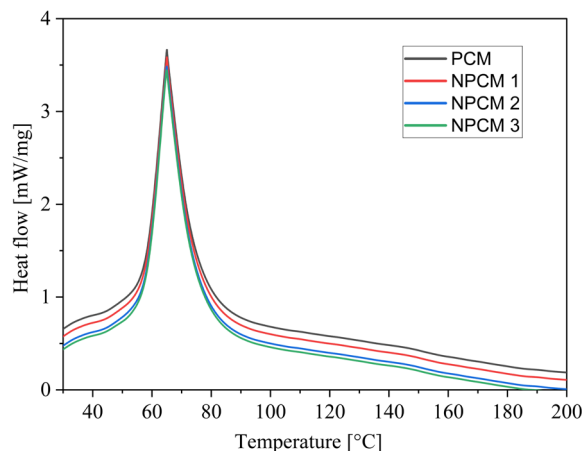


**Fig. 7.** *DSC curves of PCM and NPCM composites*

The DSC data of the samples are listed in Table 2. The melting latent heat capacity of the base PCM was 201.5 J/g. As expected, the latent heat capacity of NPCM composites containing graphene nanoparticles limited to 3 wt.% did not reduce much. Specifically, a reduction in the latent heat capacity of 1.08 %, 2.4 %, and 3.52 % was observed for NPCM 1, NPCM 2, and NPCM 3 composites, respectively. The small reduction in the heat storage capacity was due to the addition of nanoparticles in PCM [34]; for the same quantity

of the sample, the nanoparticles occupy some volume in place of PCM resulting in a drop in the latent heat capacity of the NPCM composites. In contrast, the phase transition curve of PCM and NPCM composites had only a single peak within the defined temperature range, and there were no indications of solid-solid secondary peaks. This observation demonstrates that the obtained PCM was in a pure form with negligible contaminants and had thermally stable phase change properties.

It was clear from the Table 2 data that the temperature that characterizes the melting was not markedly affected in the presence of nanographene in PCM. It was noted that the onset and peak melting temperatures of the PCM and NPCM composites were around 58 ˚C and 65 ˚C. This observation was a piece of significant evidence that the prepared NPCM composites could be used at the desired application temperature of 65 ˚C.

Fig. 8 depicts the TGA curve for the PCM and the NPCM composites, which shows that the mass loss has taken place in a single-step decomposition for all the samples. The steep decline curve indicates that the mass loss in PCM and NPCM composites are at very close proximities. As listed in Table 2, the onset thermal decomposition temperatures for PCM, NPCM 1, NPCM 2, and NPCM 3 composites were 183.6 ˚C, 194.7 ˚C, 195.4 ˚C, and 197 ˚C, respectively, which increases with an increase in the graphene mass concentration in the base PCM and follows a linear incremental trend with graphene concentration. The onset decomposition temperature for NPCM 3 composite was about 13 ˚C higher than the base PCM.

It was noticed that the onset degradation temperature of the prepared NPCM composites was higher than that of the PCM, indicating that the NPCM composites had relatively greater thermal stability. The better thermal stability of NPCM composites was linked to graphene nanoparticles' chemical inertness

and its dominance in constructing the thermal barrier (i.e., retardation against the temperature) [35], which prolongs the thermal decomposition″temperature of the NPCM composites. The complete decomposition of the PCM in all the NPCM composites occurs near 300 °C, whereas the graphene in NPCM 1, NPCM 2, and NPCM 3 composites remained undecomposed at this temperature. The final mass of each NPCM composite was near the initial mass of nanographene loaded in the composites.
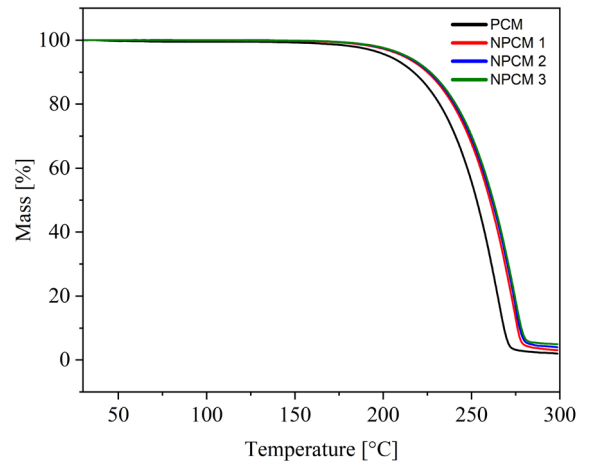


**Fig. 8.** *TGA curves of PCM and NPCM composites*

## 3 CONCLUSIONS

The experimental investigations on the thermal characterization of the prepared NPCM composites regarding its applicability for TES integrated domestic SWH have been presented in this article. The properties (i.e., microstructure, graphene presence, chemical characteristics, crystal structures, thermal conductivity) and thermal energy storage characteristics of the PCM and the NPCM composites

**Table 2.** *Thermal conductivity and DSC – TGA data of the PCM and the NPCM composites*

| Samples | Thermal conductivity, $k$ [W/(m·K)] | | Percentage improved in $k$ [%] | | Melting onset temperature [˚C] | Melting peak temperature [˚C] | Latent heat (LH) capacity [J/g] | Percentage reduced in LH [%] | Decomposition temperature [˚C] |
|---|---|---|---|---|---|---|---|---|---|
| | Solid | Liquid | Solid | Liquid | | | | | |
| PCM | 0.181 | 0.133 | - | - | 58.68 | 65.30 | 204.50 | - | 183.60 |
| NPCM 1 (99 wt.% PCM + 1 wt.% graphene) | 0.386 | 0.234 | 113.26 | 75.94 | 58.25 | 65.28 | 202.30 | 1.08 | 194.70 |
| NPCM 2 (98 wt.% PCM + 2 wt.% graphene) | 0.495 | 0.312 | 173.48 | 134.59 | 58.00 | 65.15 | 199.60 | 2.40 | 195.40 |
| NPCM 3 (97 wt.% PCM + 3 wt.% graphene) | 0.579 | 0.348 | 219.89 | 161.65 | 57.87 | 65.11 | 197.30 | 3.52 | 197.00 |

were investigated using their respective instruments. The key findings are summarized as follows:

1. The homogeneous dispersion of graphene and rougher protuberance in NPCM composites was observed via SEM analysis, ensuring the acceptable dispersion and strong embedment of graphene in PCM forms additional heat conduction paths inside the PCM network.

2. The presence of graphene in all the NPCM composites was confirmed using a Raman spectrometer.

3. The FTIR and XRD analysis results confirmed that the addition of nanographene does not affect the chemical structures and crystal structure of the base PCM, meaning that the PCM and nanographene in NPCM composites have only a physical connection where the graphene acts as a thermal conductivity enhancer.

4. Every 1 wt.% increase in graphene content in PCM resulted in a notable increase in the thermal conductivity of the prepared NPCM composites.

5. According to DSC analysis, the prepared NPCM composites had melting characteristics similar to the base PCM. The onset and peak melting temperatures for all the samples were around 61 °C and 73 °C, respectively, demonstrating that the selected PCM and NPCM composites would be ideal for the proposed application's temperature requirement.

6. Compared to the base PCM, there was a significant increase in the thermal conductivity of 219.89 % and 161.65 % in the solid and liquid states, respectively, and an insignificant drop in latent heat capacity of about 3.52 % was noted for the NPCM 3 composite. The significant increase in thermal conductivity of NPCM composites overshadows the minor decrease in their latent heat capacity.

7. The TG analysis demonstrated that the temperature at which the NPCM composites began to decompose increased linearly with increasing graphene mass fraction in the PCM. All the NPCM composites showed greater thermal stability when compared to the PCM because chemically inert graphene in NPCM composites had acted as a thermal barrier, increasing the thermal degradation temperature of the NPCM composites.

The investigations mentioned above demonstrate that the dispersion of the graphene nanoparticles in the fatty acid-based PCM is a viable option for increasing the PCM's thermal conductivity. Due to the increased thermal conductivity of the NPCM composites, the rate of melting and solidification during charging and discharging cycles could be accelerated, and this phenomenon could improve the overall performance of the NPCM-based LHTES system. Therefore, the proposed NPCM composites could be the best alternative to the conventional paraffin wax PCM for TES-integrated domestic SWHs.

The TES integrated SWH system could completely melt the NPCM composites faster than the base PCM with the available solar energy. For the maximum utilization of the available solar energy, the NPCM-based TES system's volume capacity could be increased, as the charging duration is reduced, allowing a greater quantity of NPCMs to be used. As a result, the maximum potential of latent heat capacity of NPCMs could be utilized to store additional thermal energy in it. From the application perspective, this advantage would enable the SWHs to deliver additional hot water at the desired temperature. However, the envisaged application of the proposed NPCM composites is not limited to TES integrated SWHs, they could also potentially be employed for TES integrated low-temperature waste heat recovery, and electronic thermal management applications.

Furthermore, to ascertain the thermal behaviour of the NPCMs in the longer run, performing accelerated thermal cycling tests is required. Also, to investigate the real-time behaviour of the NPCMs from an SWH perspective, it is necessary to conduct intricate studies with solar thermal energy.

## 4 ACKNOWLEDGEMENTS

## 8 REFERENCES

[1] Wray, P. (2008). Solar power. *American Ceramic Society Bulletin*, vol. 87, no. 7, p. 31-33, **DOI:10.1016/B978-0-08-102631-1.00013-4**.

[2] Singh, S., Anand, A., Shukla, A., Sharma, A. (2021). Environmental, technical and financial feasibility study of domestic solar water heating system in India. *Sustainable Energy Technologies and Assessments*, vol. 43, art. ID 100965, **DOI:10.1016/j.seta.2020.100965**.

[3] Pan, T., Wu, S., Dai; E., Liu.Y. (2013). Estimating the daily global solar radiation spatial distribution from diurnal temperature

ranges over the tibetan plateau in China. *Applied Energy*, vol. 107, p. 384-393, **DOI:10.1016/j.apenergy.2013.02.053**.

[4] Cabeza, L.F. (2012). Thermal energy storage. *Comprehensive Renewable Energy*, vol. 3, p. 211-253, **DOI:10.1016/B978-0-08-087872-0.00307-3**.

[5] Ho, C.J., Gao,J.Y. (2009). Preparation and thermophysical properties of nanoparticle-in-paraffin emulsion as phase change material. *International Communications in Heat and Mass Transfer*, vol. 36, no. 5, p. 467-470, **DOI:10.1016/j.icheatmasstransfer.2009.01.015**.

[6] Ma, G., Sun, J., Zhang, Y., Jing, Y., Jia, Y. (2019). A novel low-temperature phase change material based on stearic acid and hexanamide eutectic mixture for thermal energy storage. *Chemical Physics Letters*, vol. 714, p. 166-171, **DOI:10.1016/j.cplett.2018.11.003**.

[7] Sari, A. (2012). Thermal energy storage properties of mannitol-fatty acid esters as novel organic solid-liquid phase change materials. *Energy Conversion and Management*, vol. 64, p. 68-78, **DOI:10.1016/j.enconman.2012.07.003**.

[8] Zsembinszki, G., Fernández, A.G., Cabeza, L.F. (2020). Selection of the appropriate phase change material for two innovative compact energy storage systems in residential buildings. *Applied Sciences*, vol. 10, no. 6, art. ID 2116, **DOI:10.3390/app10062116**.

[9] Fazilati, M.A., Alemrajabi, A.A. (2013). Phase change material for enhancing solar water heater, an experimental approach. *Energy Conversion and Management*, vol. 71, p. 138-145, **DOI:10.1016/j.enconman.2013.03.034**.

[10] Al-Kayiem, H.H. Lin, S.C. (2014). Performance evaluation of a solar water heater integrated with a PCM nanocomposite TES at various inclinations. *Solar Energy*, vol. 109, p. 82-92, **DOI:10.1016/j.solener.2014.08.021**.

[11] Mandal, S.K., Kumar, S., Singh, P.K., Mishra, S.K., Bishwakarma, H., Choudhry, N.P., Nayak, R.K., Das, A.K. (2019). Performance investigation of CuO-paraffin wax nanocomposite in solar water heater during night. *Thermochimica Acta*, vol. 671, p. 36-42, **DOI:10.1016/J.tca.2018.11.003**.

[12] Zavrl, E., Zupanc, G., Stritih, U., & Dovjak, M. (2020). Overheating reduction in lightweight framed buildings with application of phase change materials. *Strojniski vestnik - Journal of Mechanical Engineering*, vol. 66, no. 1, p. 3-14, **DOI:10.5545/sv-jme.2019.6244**.

[13] Yuan, Y., Zhang, N., Tao, W., Cao, X., He, Y. (2014). Fatty acids as phase change materials: A review. *Renewable and Sustainable Energy Reviews*, vol. 29, p. 482-498, **DOI:10.1016/j.rser.2013.08.107**.

[14] Duquesne, M., Mailhé, C., Doppiu, S., Dauvergne, J.L., Santos-Moreno, S., Godin, A., Fleury, G., Rouault, F., Del Barrio, E.P.. (2021). Characterization of fatty acids as biobased organic materials for latent heat storage. *Materials*, vol. 14, no. 16, art. ID 4707, **DOI:10.3390/ma14164707**.

[15] B, E.J., A, V.A.. (2020). Characterisation and stability analysis of eutectic fatty acid as a low cost cold energy storage phase change material. *Journal of Energy Storage*, vol. 31, srt. Id 101708, **DOI:10.1016/j.est.2020.101708**.

[16] Narayanan, S.S., Kardam, A:, Kumar, V., Bhardwaj, N., Madhwal, D., Shukla, P., Kumar, A., Verma, A., Jain, V.K.

(2017). Development of sunlight-driven eutectic phase change material nanocomposite for applications in solar water heating. *Resource-Efficient Technologies*, vol. 3, no. 3, p. 272-279, **DOI:10.1016/j.reffit.2016.12.004**.

[17] Ling, Z., Chen, J., Xu, T., Fang, X., Gao, X:, Zhang, Z. (2015). Thermal conductivity of an organic phase change material/ expanded graphite composite across the phase change temperature range and a novel thermal conductivity model. *Energy Conversion and Management*, vol. 102, p. 202-208, **DOI:10.1016/j.enconman.2014.11.040**.

[18] Shah, K.W.. (2018). A review on enhancement of phase change materials - A nanomaterials perspective. *Energy and Buildings*, vol. 175, p. 57-68, **DOI:10.1016/j.enbuild.2018.06.043**.

[19] Kibria, M.A., Anisur, M.R., Mahfuz, M.H., Saidur, R., Metselaar, I.H.S.C. (2015). A review on thermophysical properties of nanoparticle dispersed phase change materials. *Energy Conversion and Management*, vol. 95, p. 69-89, **DOI:10.1016/j.enconman.2015.02.028**.

[20] Fan, L.W., Fang, X., Wang, X., Zeng, Y., Xiao, Y.Q., Yu, Z.T., Xu, X., Hu, Y.C., Cen, K.F. (2013). Effects of various carbon nanofillers on the thermal conductivity and energy storage properties of paraffin-based nanocomposite phase change materials. *Applied Energy*, vol. 110, p. 163-172, **DOI:10.1016/J.apenergy.2013.04.043**.

[21] Qureshi, Z.A., Ali, H.M., Khushnood, S. (2018). Recent advances on thermal conductivity enhancement of phase change materials for energy storage system: A review. *International Journal of Heat and Mass Transfer*, vol. 127, p. 838-856, **DOI:10.1016/j.ijheatmasstransfer.2018.08.049**.

[22] Renteria; J.D., Nika, D.L., Alexander A. Balandin, A.A. (2014). Graphene thermal properties: Applications in thermal management and energy storage. *Applied Sciences*, vol. 4, no. 4, p. 525-547, **DOI:10.3390/app4040525**.

[23] Zeng, Y., Fan, L.W., Xiao, Y.Q., Yu, Z.T., Cen, K.F. (2013). An experimental investigation of melting of nanoparticle-enhanced phase change materials (NePCMs) in a bottom-heated vertical cylindrical cavity. *International Journal of Heat and Mass Transfer*, vol. 66, p. 111-117, **DOI:10.1016/j.ijheatmasstransfer.2013.07.022**.

[24] Zou, D., Ma, X., Liu, X., Zheng, P., Hu, Y. (2018). Thermal performance enhancement of composite phase change materials (PCM) using graphene and carbon nanotubes as additives for the potential application in lithium-ion power battery. *International Journal of Heat and Mass Transfer*, vol. 120, p. 33-41, **DOI:10.1016/j.ijheatmasstransfer.2017.12.024**.

[25] Xiang, J., Drzal, L.T. (2011). Investigation of exfoliated graphite nanoplatelets (xGnP) in improving thermal conductivity of paraffin wax-based phase change material. *Solar Energy Materials and Solar Cells*, vol. 95, no. 7, p. 1811-1818, **DOI:10.1016/j.solmat.2011.01.048**.

[26] Kim, S.C., Prabakaran, R., Sakthivadivel, D:, Thangapandian, N., Bhatia, A., Kumar, P.G. (2020). Thermal transport properties of carbon-assisted phase change nanocomposite. *Fullerenes Nanotubes and Carbon Nanostructures*, vol. 28, no. 11, p. 925-933, **DOI:10.1080/1536383X.2020.1786814**.

[27] Ali, M.A., Fayaz, Viegas, R.F., Kumar, M.B.S., Kannapiran, R.K., Feroskhan, M. (2019). Enhancement of heat transfer in paraffin wax PCM using nano graphene composite for

industrial helmets. *Journal of Energy Storage*, vol. 26, art. ID 100982, **DOI:10.1016/j.est.2019.100982**.

[28] Harikrishnan, S., Kalaiselvam, S. (2012). Preparation and thermal characteristics of CuO-oleic acid nanofluids as a phase change material. *Thermochimica Acta*, vol. 533, p. 46-55, **DOI:10.1016/j.tca.2012.01.018**.

[29] Singh, N.P., Gupta, V.K., Singh, A.P., Sapra, B. (2021). Synergistic effects of graphene nanoplatelets and NH2-MWCNTs on cryogenic mechanical properties of epoxy nanocomposites. *Polymer Testing*, vol. 94, art. ID 107032, **DOI:10.1016/j.polymertesting.2020.107032**.

[30] Zhang, L., Zhang, P., Wang, F., Kang, M., Li, R., Mou, Y., Huang, Y. (2016). Phase change materials based on polyethylene glycol supported by graphene-based mesoporous silica sheets. *Applied Thermal Engineering*, vol. 101, p. 217-223, **DOI:10.1016/j.applthermaleng.2016.02.120**.

[31] Lin, Y:, Zhu, C., Fang, G. (2019). Synthesis and properties of microencapsulated stearic acid/silica composites with graphene oxide for improving thermal conductivity as novel solar thermal storage materials. *Solar Energy Materials and Solar Cells*, vol. 189, p. 197-205, **DOI:10.1016/j.solmat.2018.10.005**.

[32] Goli, P., Legedza, S., Dhar, A., Salgado, R., Renteria, J., Balandin, A.A.. (2014). Graphene-enhanced hybrid phase change materials for thermal management of Li-ion batteries. *Journal of Power Sources*, vol. 248, p. 37-43, **DOI:10.1016/j.jpowsour.2013.08.135**.

[33] Wu, S.Y., Wang, H., Xiao, S., Zhu, D.S. (2012). An investigation of melting/freezing characteristics of nanoparticle-enhanced phase change materials. *Journal of Thermal Analysis and Calorimetry*, vol. 110, p. 1127-1131, **DOI:10.1007/s10973-011-2080-x**.

[34] Liu, P., Gu, X., Rao, J., Liu, S., Wang, B., Bian, L. (2020). Preparation and thermal properties of lauric acid/raw fly ash/carbon nanotubes composite as phase change material for thermal energy storage. *Fullerenes Nanotubes and Carbon Nanostructures*, vol. 28, no. 11, p. 934-944, **DOI:10.1080/1536383X.2020.1786815**.

[35] George, M., Pandey, A.K., Rahim, N.A., Tyagi, V.V., Shahabuddin, S., Saidur, R. (2020). A novel polyaniline (PANI)/ paraffin wax nano composite phase change material: Superior transition heat storage capacity, thermal conductivity and thermal reliability. *Solar Energy*, vol. 204, p. 448-458, **DOI:10.1016/j.solener.2020.04.087**.